A TECHNIQUE FOR PREDICTING THE MUON INDUCED UPSET CROSS SECTION IN SUBMICRON MOS DEVICES USING PROTON TESTS AND SIMULATION

By

James Michael Trippe

Thesis

Submitted to the Faculty of the

Graduate School of Vanderbilt University

in partial fulfillment of the requirements

for the degree of

Master of Science

in

Electrical Engineering

August, 2014

Nashville, Tennessee

Approved:

Marcus H. Mendenhall, Ph.D.

Robert A. Reed, Ph.D.

To my mother and father, Ann Reichheld and Charles Trippe, and to Rain

ACKNOWLEDGEMENTS

This work would not have been possible without the financial support of the Defense Threat Reduction Agency or Cisco Systems. Additionally I would like the thank Dr. Daniel Fleetwood, the department chair of Electrical Engineering & Computer Science at Vanderbilt University, for his support while working with the Radiation Effects and Reliability group. I would like to thank my thesis advisor, Dr. Marcus Mendenhall, for his assistance with this work and with my other endeavors as a graduate student at Vanderbilt. He has been infinitely patient with me as I learned the material required to pursue my goals and was always there when I needed him. As my mentor, he has shown me what it means to be dedicated to scientific research. My second reader, Dr. Robert Reed, has also been an inspiration throughout my career so far at Vanderbilt. I especially appreciate his challenging my work when it needed to be. Other faculty members, especially Dr. Robert Weller and Dr. Ronald Schrimpf, have provided me with insight into physics, computer science, and presentation style that will stay with me my entire career.

I also thank my parents, Ann Reichheld and Charles Trippe, for their support over the many years I've been in school. They have always been my first role models and I emulate them in every sense I am able. I'd like to thank Rain, who has been by my side all this time during my graduate career and who has helped me focus my life. Finally, I wish to thank my siblings, Doug and Marta, who have been inspirations themselves despite being younger.

TABLE OF CONTENTS

Page

DEDICATION ii

ACKNOWLEDGEMENTS iii

LIST OF TABLES v

LIST OF FIGURES vi

Chapter

I. Introduction 1

II. Motivation 2
   Terrestrial Muon Induced Upsets 3
   Muon and Proton Beams 4

III. Background 6
   Mechanisms of Muon and Proton Induced Upsets 6
   Simulation Tools 8

IV. Approach 9
   Method 1: LET constant within SV 9
   Method 2: LET varies within SV 9
   Conditions for choosing between Method 1 and Method 2 10
   Mapping from proton energies to muon energies 17
   Propagating from energy deposition to upset rate 17
   Determine the muon upset rate using the methods 18

V. Proton Testing 20

VI. Simulation Concerns Using MRED 22

VII. Validation 24

VIII. Sample simulation and usage of the methods 28

IX. Inhomogeneous BEOL Structures 32

X. Method 2 with TRIM 34

XI. Future Work 37

XII. Conclusion 39

REFERENCES 40

APPENDIX 42

LIST OF TABLES

Table **Page**

1. Change in consistency of ratio proton to muon energy deposition depending on source 28

2. Sample Device - Velocity matched proton energies for given muon energies.................................... 29

3. Sample Device - Comparison of proton and muon energy deposition in the 500 keV muon case.. 30

4. Sample Device - Comparison of proton and muon energy deposition in the 1 MeV muon case.. 31

5. Ratio of proton to muon energy depositions for select energies incident on the device presented in Fig. 14.. 33

LIST OF FIGURES

Figure | Page

1. Terrestrial particle environment over New York City and muon upset rates for 65 nm, 45nm, and 40 nm SRAMs 2
2. Muon stopping power in Cu 5
3. Experimental (top) and simulated (bot) energy deposition counts for a 500 µm thick surface barrier detector, taken at the TRIUMF muon beam facility 7
4. The overall methodology of testing for muon induced upsets with protons 9
5. TRIM simulation of muons incident on a simple test device 12
6. Velocity matched muon (1 MeV) and proton (8.9 MeV) energy deposition in a silicon volume 13
7. Proton energy as a function of muon energy for which both particles deposit the same amount of energy in a thin volume positioned after the noted SiO2 BEOL thickness 14
8. Muons at sea level and after being transported through 10 cm of concrete 18
9. Outline of proton hardness assurance testing procedure 21
10. Device geometry used for several of the examples in Validation-Simulation 24
11. Results demonstrating the relationship between average energy deposition per cell. 25
12. Ratio of proton and muon energy depositions as a function of sensitive volume depths 26
13. Model of the device used in the sample simulations 28
14. Inhomogeneous stack of materials used in the following simulations 32
15. TRIM outputs comparing ionization in the structure illustrated in Fig. 13 for 500 keV muons and 2.8 MeV protons 34
16. Muon SEU results for three 28 nm SRAMs across several incident muon energies. 37

CHAPTER I

INTRODUCTION

Single-event upsets (SEUs) are a primary concern for radiation induced circuit failures in modern terrestrial applications .SEUs are caused when charged particles strike a transistor and generate enough charge to cause a change in the state of the device. [1] Muons are one of the most numerous terrestrial particle species, making up a large percentage of the high energy particles reaching the Earth's surface as cosmic radiation. Previous work has shown that at technologies as large as 45 nm, muon induced upsets at terrestrial energies become common enough to negatively impact circuit performance. [2] Since then, significant work has been done to understand devices' responses to high energy muons. However, the current methodology to test parts for muon SEU immunity involves a rigorous and time-consuming testing procedure. The goal of this work is to reduce testing to only protons and evaluate the device's response to muons through Monte Carlo simulation techniques. Examples are presented for the use of the methods in this paper for selecting proton energies for experimentation. Guidance is also provided to navigate the user around common pitfalls with the methods, such as the effects of certain simulation options or the effects of certain device structures. At the end of the report, an alternate methodology is discussed that, while faster and simpler to implement than the other methods, decreases the accuracy of the measurement.

The focus throughout this work will be on Monte Carlo Radiative Energy Deposition (MRED) and Transport of Ions in Matter (TRIM) as the tools of choice for performing the simulations associated with the methods. However, any code that can accurately determine the energy deposition of an ion in a localized region of a stack of materials could be used in their place.

CHAPTER II

MOTIVATION

Terrestrial Muon Induced Upsets

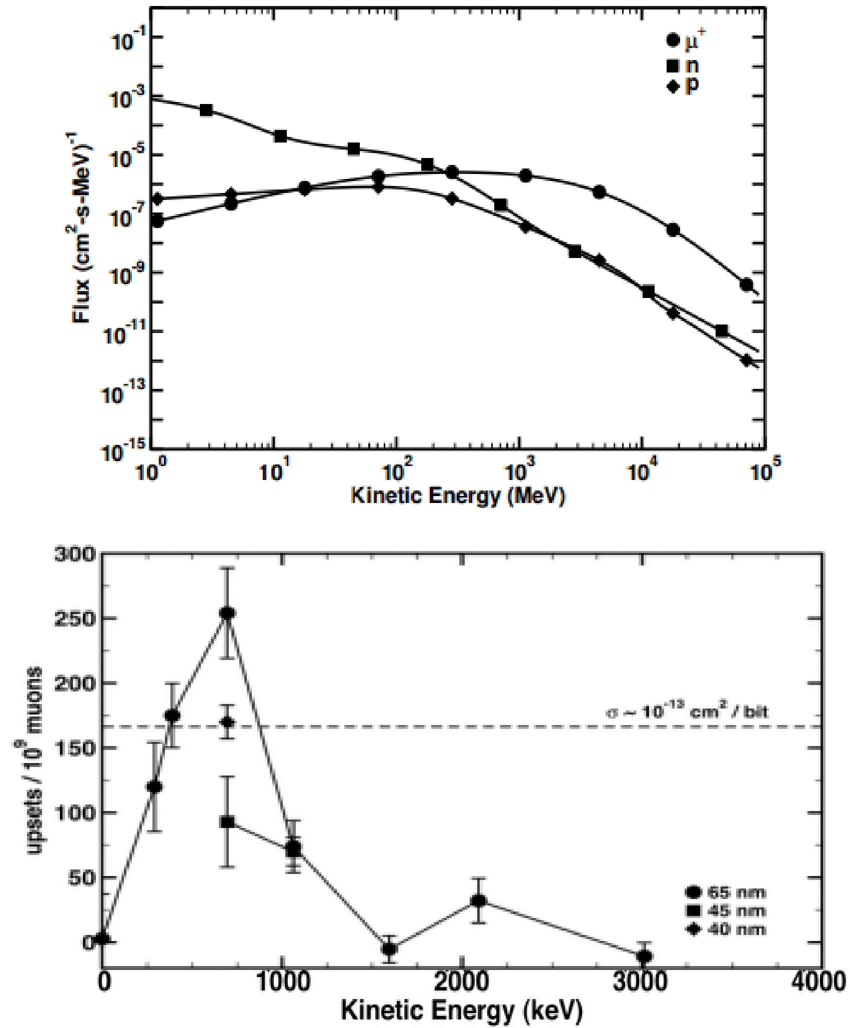

Figure 1a (top): Terrestrial particle environment over New York City [3]

Figure 1b (bottom): Muon upset rates for 65 nm, 45nm, and 40 nm SRAMs [2]

Cosmic ray particles entering the atmosphere interact in the air and produce a shower of products that rain down to the Earth's surface. Among those are muons, which despite their charge and short lifetime, can reach the Earth's surface due to the effects of Lorentz contraction. The distribution of particle energies at sea level over New York City is shown in Fig. 1a. Muons are the most common particle in the cosmic ray shower, with a flux that peaks near 4 GeV. Sierawski *et al.* have shown that submicron technology is vulnerable to muon induced upsets as shown in Fig. 1b. [2] Integrating these facts, it becomes apparent that even terrestrial applications are vulnerable to muon induced upsets. However, finding ways to characterize devices' response to these particles poses a significant challenge.

Muon and Proton Beams

There are only a handful of facilities around the world capable of producing muons in a controlled laboratory setting. Institutions capable of generating muon beams mostly cater only to academic enterprises and applications for beam time must be approved through a proposal process. Another issue with muon beams is that the techniques used to produce them create significant spreading in the energy spectrum. For example, the muon beam at TRIUMF is created by pion decay within a target, which can lead to up to a peak with a full width of half max of up to 10% of the mean beam energy. [4] Any spread in the energy distribution must be accounted for in experiments and can require additional beam degradation to accurately determine each muon energy's contribution to the total upset cross section. Proton beams, on the other hand, are much more available. Many academic institutions have their own proton beams, and many of these give time to academics readily or sell time to corporations. Additionally, since protons can be generated from directly ionizing hydrogen, beams such as those produced by a Pelletron accelerator tend to be nearly monoenergetic.

This paper demonstrates a way to accurately predict muon induced errors with proton experiments and Monte Carlo simulations that will forego the more difficultly-accessed muon beams in favor of proton

beams. This is especially of interest for corporations intending to test their parts for vulnerability to ionizing muon radiation, since previously they have been unable to. At high energies, a positively charged muon will behave identically to a proton with equal velocity and linear energy transfer (LET). The method is split into two cases, one that requires less device information than the other. The first focuses on particles residing in the power law governed region of the stopping power curve within the Bethe-Bloch region as shown in Fig. 2. Here both protons and muons behave as identically charged particles travelling through a solid material at the same speed and have nearly constant LET. The prediction of the muon energy deposition will be reduced to only using proton tests by taking advantage of the similarity between the proton's and muon's energy deposition. The other important region is the Andersen-Ziegler region where the particle begins stopping and losing energy. At these energies, the muon's LET changes rapidly as a function of distance, making it much more difficult to predict the energy deposition with protons (since they stay at nearly the same LET well past the muon Bragg peak). This requires a different technique, explained later in the paper, which involves using simulations to derive the proton LET to match the expected muon LET within the sensitive volume.

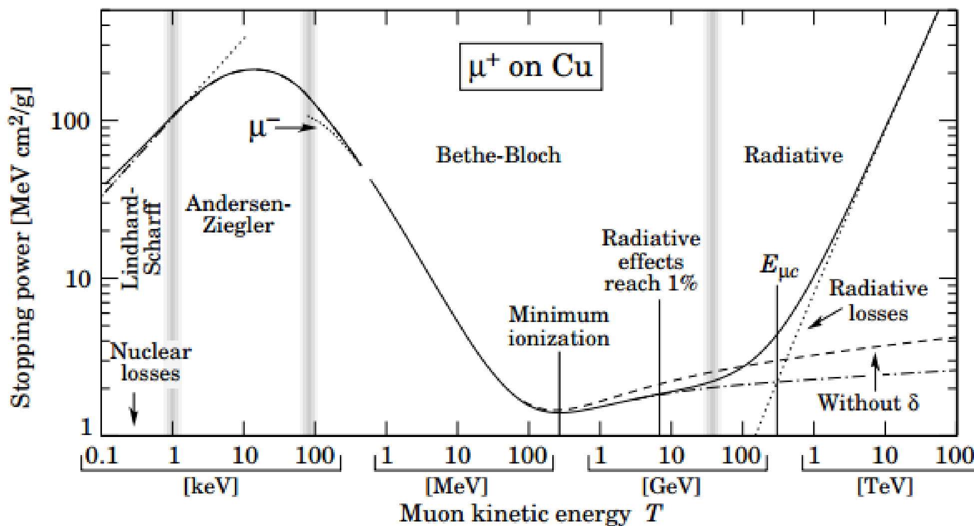

Figure 2: Muon stopping power in Cu [5]

Vanderbilt has both a Pelletron accelerator and a Monte Carlo simulation tool called MRED (Monte Carlo Radiative Energy Deposition). Researchers working at the university who desire to test parts for vulnerability to muon induced upsets will find the work in this paper applicable. While some general techniques will be presented, many of the methods presented here focus on the use of Vanderbilt's Pelletron and MRED code. The Vanderbilt Pelletron produces a nearly monoenergetic beam that can be used to easily select proton LETs to be tested. According to data collected from that beam, the full width at half max of the beam energy spectrum can be as low as 100 keV for 1.8 MeV protons. MRED contains all the physics tools needed to confirm that the cross section measured in the proton tests correspond to the cross section of muons of the same LET. These two tools are the backbone of the methods presented later in the paper.

CHAPTER III

BACKGROUND

Mechanisms of Muon and Proton Induced Upsets

Sierawski has identified low energy proton and muon SEUs as a concern for sub 100 nm technology. Note from Fig. 1a that the muon flux peaks at about 4 GeV, an energy level that is far from the upset threshold for the parts in Fig. 1b. However, after penetrating some material, the energy will be lost to Coulomb interactions. By the time it reaches the sensitive volume, the muon will have lost significant energy. Simulations have shown that after passing through 10 cm of concrete, the muon flux between 1 keV and 2 MeV was nearly constant at 10^{-6} cm^{-2}-s^{-1}-MeV^{-1}. It was also found that low energy stopping muons contribute most to the SEU rate, as the LET of muons in the Bragg peak is much greater than muons with higher energies. Thus, after the energy losses experienced in the concrete, there remain a significant number of low energy muons with LETs high enough to cause upsets. Due to these factors, the actual amount of air, concrete, or even back end of line (BEOL) does not significantly change the low energy tail. [3]

Note that for the purposes of describing this method positive muons were used, as negative muons will become captured by nuclei in the material as they slow down. Thus, negative muons have radically different energy deposition mechanisms in the Andersen-Ziegler region compared to protons, which behave similarly to positively charged muons. In addition, they are more difficult to produce in muon beams due to tendencies to get swept up in the production target.

Muons have several other characteristics that distinguish them from protons that must be considered when attempting to make the comparison between the two. First, muons have a mass of 105 MeV compared to mass of 938 MeV for proton. Two identically charged particles moving through a material

with the same velocity will, on average, have the same electronic stopping power. To apply one of the methods presented in this paper, the proton and muon LETs must be matched accordingly within the sensitive volume (SV). Thus, to match both particles' velocity, the energy of the proton must be chosen according to Eqn. 1.

Equation 1: $E_p = E_\mu * \frac{m_p}{m_\mu}$

When the proton and muon energies are matched, the particle's LET should be identical.

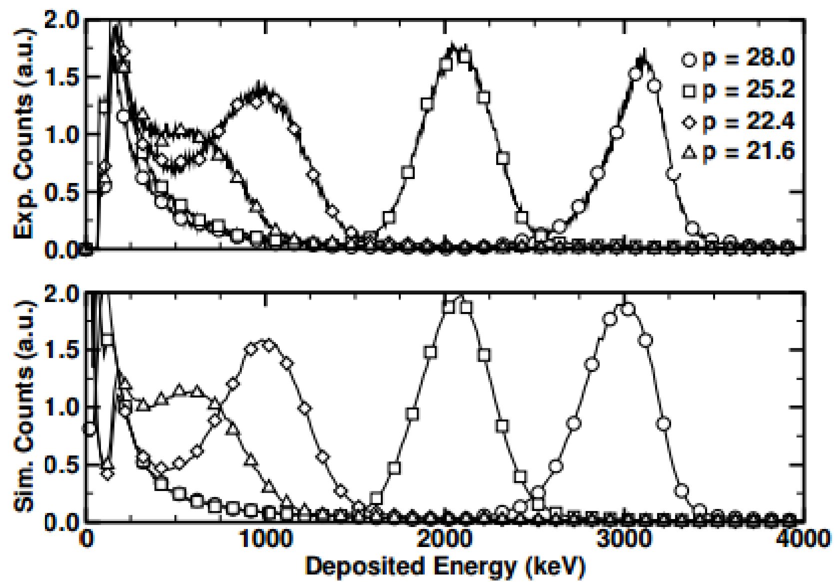

Figure 3: Experimental (top) and simulated (bot) energy deposition counts for a 500 µm thick surface barrier detector, taken at the TRIUMF muon beam facility [2]

Another potential concern for muons is the energy produced by the muon's decay. A muon has an average lifetime of 2.2 µs, which is on an order of magnitude much larger than the transient pulse from the upset. Sierawski *et al.* showed that the energy released by the positive muon's decay into the product positron and neutrinos doesn't cause SEUs. [2] Note the results in Fig. 3 give the number of counts as a function of energy deposition in a surface barrier detector for the M20 muon beam at

TRIUMF. The larger energy peaks are caused by muons traveling through air gaps and the mylar window. The wide peak at 500 keV is caused by energy deposition from decays, and is significantly less than the energy deposition from direct ionization. However, in the future, smaller technologies may become vulnerable to this decay process. The implications of this are discussed in Section XI, though for now the contribution of muon decay will be ignored.

Simulation Tools

MRED was the simulation platform of choice both to demonstrate and validate the methods presented here [6]. MRED is a Geant4-based radiation transport code that contains the necessary physical models to accurately compute the interactions of a particle with a target material. Using the Monte Carlo simulation technique, MRED can generate large numbers of particles that interact in the target material according to probabilities derived from the underlying physics. Over a large number of strikes, a distribution of the number of events for each value of energy deposition will emerge. The geometry of the target can be described in great detail, from the materials used in the BEOL to the sensitive volume depth. MRED contains all the tools necessary for a simulation tool to validate the methods proposed here for predicting muon energy deposition with protons.

In this paper, MRED simulation results are presented as energy deposited within the sensitive volume of a given device model. Sample code is given in the Appendix. This code determines the device model used, typically given as a stack of layered materials approximating a BEOL, SV layer, and substrate. The SV region where the energy deposition is counted is determined by a box in x,y,z. Within that region, the energy deposited is averaged per particle. The particle beam is defined by arguments provided from the Linux command line. These parameters include particle energy, number of simulation counts, beam angle, and spatial sampling. The dependence on the simulation results on each of these is covered in sections VI and VII. Typical particle counts for a simulation are 100,000 striking the sensitive volume.

CHAPTER IV

APPROACH

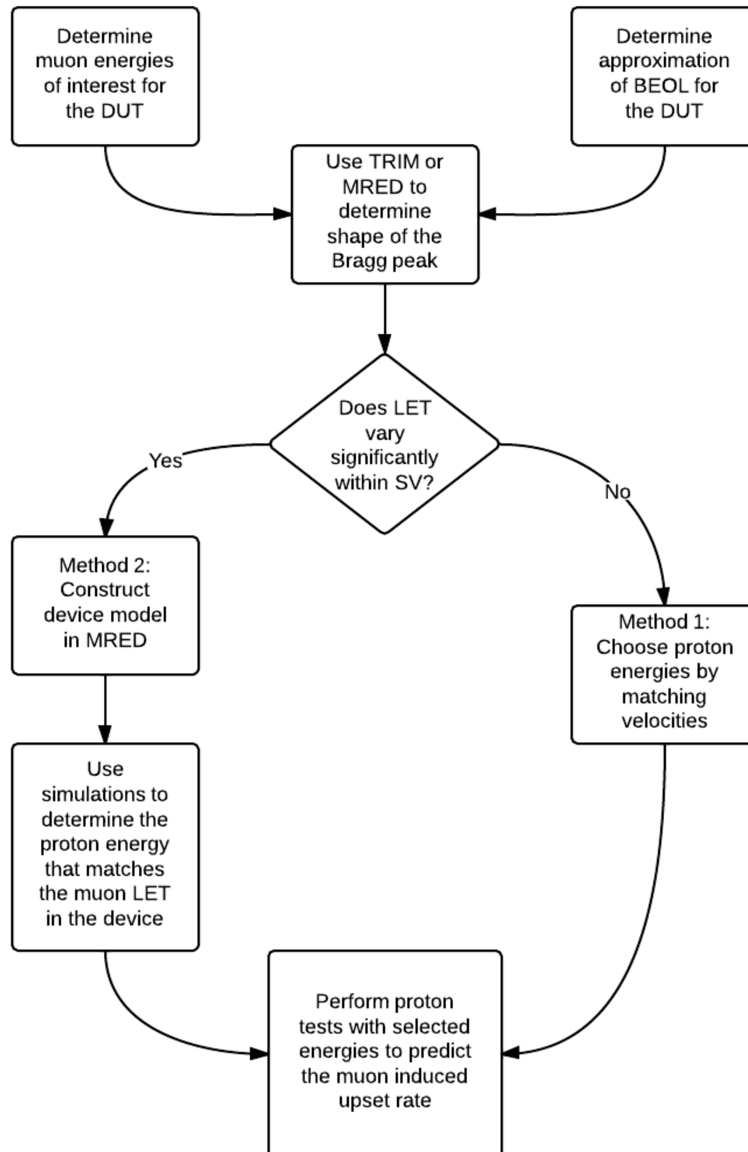

Figure 4: The overall methodology of testing for muon induced upsets with protons

This section will outline the methodology for comparing muon and proton energy depositions. The main criteria for predicting muon energy deposition with protons is to ensure that the test proton has the

same LET as the muon would in the sensitive volume. Two methods, one for the simple case of near constant LET and a second for the case where the LET is changing rapidly in the material can be used for the comparison. First, these two methods are presented, after which the conditions for choosing either method are discussed in detail. Validation of the process will be presented following this section in the form of simulation and experimental results. For reference, a flowchart showing the overall methodology is presented in Fig. 4.

Method 1: LET constant within SV

The first method should be chosen in the case where the sensitive volume depth is located well before the muon Bragg peak. At this point, tests can be performed such that the protons velocity is matched to the muons by using Eqn. 1. In this case the muon and proton LET will be identical and thus the deposited energy and charge will be identical. The cross section observed during proton testing would therefore be representative of the theoretical muon cross section. Since it is not necessary to perform simulations as part of this qualification method, knowledge of the exact device geometry is optional as long as the muon stops far enough after the sensitive volume that its LET is not changing significantly within the SV.

The method presented in this section corresponds to muons which deposit their energy without stopping within the sensitive volume and will be referred to "Method 1" throughout the rest of the paper.

Method 2: LET varies within SV

The second method is required if the sensitive volume is located close to or within the muon Bragg peak. To use this method, an accurate knowledge of the device geometry is required to perform simulations with a tool such as MRED or TRIM. After performing simulations to determine a plot such as in Fig. 5, the LET should be chosen at the sensitive volume depth. Then, using the same simulation, determine a

proton energy that has the same LET as the muon at this point. This is the proton energy that must be used during testing to predict the muon cross section. These proton tests should be compared against the simulation results to ensure that the model chosen was accurate. One concern is that the changing muon LET near the Bragg peak might cause an error, but results presented here demonstrate that for small sensitive volumes such as in modern technologies the muon's LET does not change significantly compared to the proton's.

The method presented in this section corresponds to muons which deposit their energy while stopping near enough to the sensitive volume that the Bragg peak produces an error greater than is tolerable for the application. It will be referred to "Method 2" throughout the rest of the paper.

Conditions for choosing Method 1 versus Method 2

The first step is to determine if the muons are stopping within the sensitive volume of the device or if they are passing through. The most accurate way to determine this is to construct a model of the device from known specifications and perform simulations of muon particle strikes. Of course, this requires a detailed knowledge of the device and a physics simulator to determine how the particle is behaving. If this not available, a rough knowledge of the BEOL will be sufficient to determine an estimate of the particle's energy deposition profile with a free tool such as Stopping Range of Ions in Matter (SRIM). Even without a perfect understanding of the physics, a reasonable estimate of the projected range of the muon will be sufficient for Method 1. Fig. 5 shows the results of a Transport of Ions in Matter (TRIM , part of the same software package as SRIM) simulation to determine the energy deposition profile of muons within the SV of a test structure. TRIM does not normalize energy deposition per unit path length to density, something that should be understood when interpreting its output. Note that in this case the muon Bragg peak is peaking near Layer 2, which is the sensitive volume for the device, implying that Method 2 should be used. More information on TRIM simulations is provided in section X. Additionally,

Buchner *et al.* have demonstrated an excellent use of free simulation tools to determine the location of a particle's Bragg peak in a stack of materials. [7]

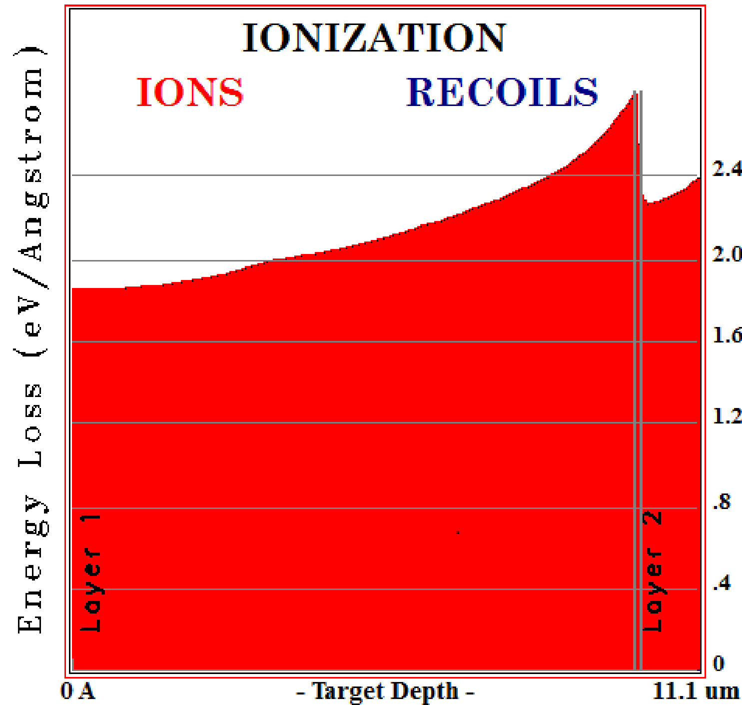

Figure 5: TRIM simulation of muons incident on a simple test device

The next step is to choose the proton energy that should be used to predict the muon's energy deposition as accurately as possible. An example from GEANT4 is shown in Fig. 6 which shows differential energy deposition as a function of distance in a 100 µm chunk of silicon. The proton and muon LETs are chosen to match closely at the surface, but the proton LET begins to undershoot the muon's LET as the muon enters the Bragg peak. The margin of error in the user's calculations is the best metric for determining which of the following two methods are best to use. For example, if the acceptable margin of error is selected to be 10%, then in Fig. 5 the maximum depth where the first method is permissible would be about 20 µm. After that point, the proton LET diverges from the muon LET by more than 10%, so the margin of error in the energy depositions will be 10% (assuming the same device geometry). This does not correspond to a 10% difference in cross section; it is the user's

responsibility to determine the critical charge of the device for that sort of calculation. If the device geometry is not well known then 20 µm might be cutting it close, but if the BEOL is 5 µm thick then even with a rough simulation it is likely fine to use Method 1 (in this specific case). If the margin of error is too great, then Method 2 must be used. Note that the first method is much easier to apply without extensive knowledge of the device, so it is preferable if possible. The methodologies for testing devices for proton induced upsets are well understood, and the techniques outlined under Proton Tests should be applied when using the proton tests to determine muon induced upsets.

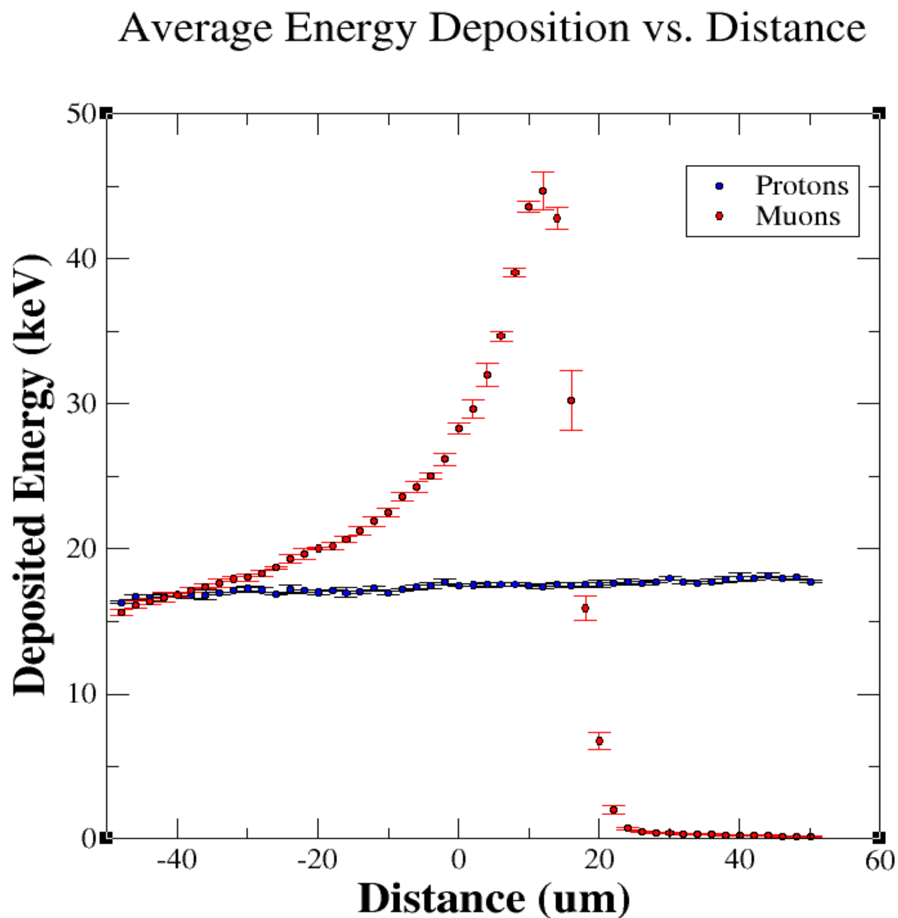

Figure 6: Velocity matched muon (1 MeV) and proton (8.9 MeV) energy deposition in a silicon volume

Consider Fig. 7, which shows the proton energy whose energy deposition matches the muon's as a function of that muon energy for three different simple BEOL structures.

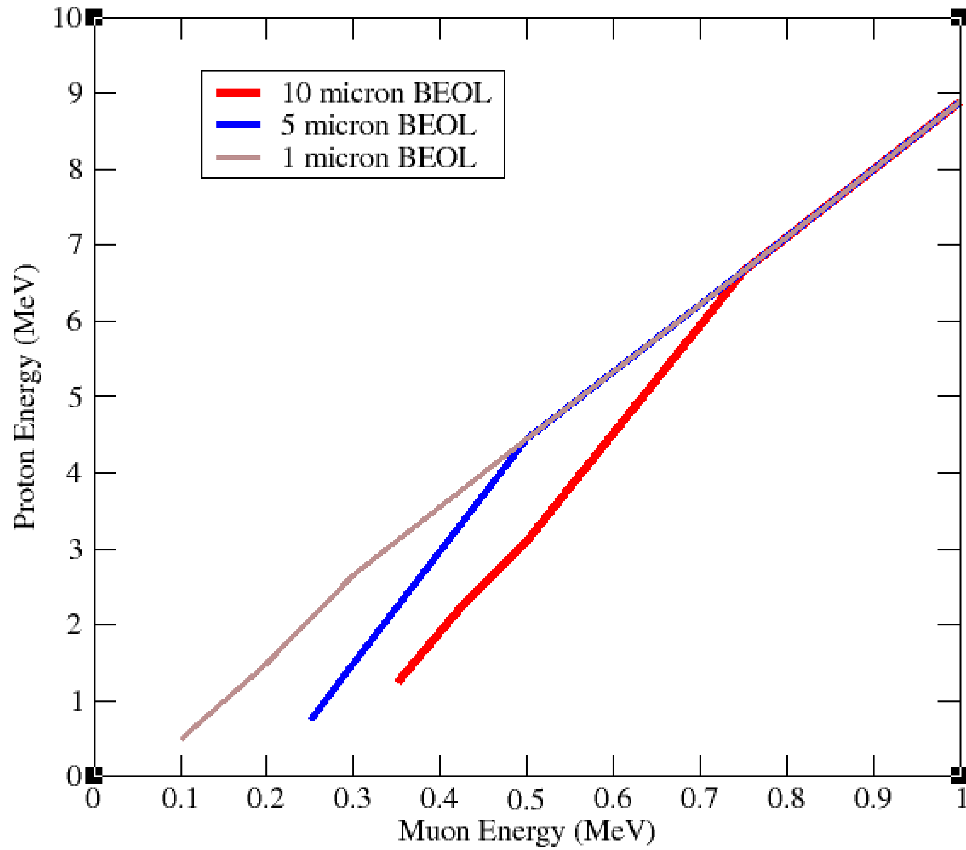

Figure 7: Proton energy as a function of muon energy for which both particles deposit the same amount of energy in a thin volume positioned after the noted SiO_2 BEOL thickness.

Note that for high energy muons (>700 keV) the relationship between the chosen proton and muon energies is linear with a slope of 8.89. This is due to the more energetic muons losing little energy in the BEOL due to their low LET, so the velocity matching technique used in Method 1 works well. However, for lower muon energies, as the muon stops the proton energy required to deposit the same amount of energy in the SV decreases compared to the velocity matched particle. Since the muon stops at higher energies in larger BEOLs, the function's deviation from the linear happens at a higher energy as well.

Thus, when testing with thicker BEOLs, method 2 is preferred to Method 1 for a larger range of muon energies compared to smaller BEOLs.

In Fig. 7, for each case there are energies where the only contributions to the energy deposition are from delta rays since the muons stop too early in the BEOL. These would occur just below the minimum muon energy shown in the plot. Typically, these events will deposit 100-1000 times less energy than even 5 MeV muons would. Thus, they can typically be ignored since they will likely not cause upsets. If for whatever reason they must be considered, method 2 will work but the proton energies chosen will often be above 100 MeV, which is often impractical.

If the knowledge of the BEOL is inaccurate, the choice of proton energy may be inaccurate. However, exact knowledge is rarely required. What matters is the product of density and depth of the materials in the BEOL. As such, metallization, oxide, and heavy metal plugs can be treated as homogenous layers by simply considering the total depth of the combination of layers of each of the materials. Small variations in the composition of these layers will have a roughly linear effect on the energy deposition in the sensitive volume. However, if enough proton energies are tested then the peak in upset cross section will still be found even with moderate variations in knowledge of the BEOL. Then, if the muon peak that it corresponds to is in question then analysis can be done after the experiment to correct the calibration between proton and muon energies. If the BEOL modeled is vastly different from the actual BEOL then finding the peak proton upset cross section may be a problem.

Another source of error in the final measurement would be the variation in energy for a proton beam. Ion beams never create a stream of monoenergetic particles; some will have energies above and below the mean. This is an area where the proton beam has a distinct advantage over a muon beam. Typically, proton beams can be made very monoenergetic compared to muon beams. In order to have a powerful enough beam, a wider selection of the muon energy ranges must be chosen compared to protons.

Additionally, due to the nature of the methods outlined here, the protons are not stopping so differences in energy deposition between the maximum and minimum would be relatively small compared to the stopping muons. Recall from Fig. 6 that that stopping particles have much larger change in LET for a change in particle energy.

Mapping from proton energies to muon energies

It is worth noting here that the methods presented here discuss going from known muon energies to proton energies for testing. Of course, it is possible to go from protons to muons as well. Say an experimenter has determined SEU rates for protons and wishes to know what muon energies each of these rates correspond to. This can be done by mapping each proton energy to a velocity matched muon energy and determining the shape of the muon Bragg peak as in chapter IV. If the energy deposition changes less than the threshold determined by the experimenter, then that proton SEU rate corresponds to a muon with the same velocity. Otherwise, simulations similar to method 2 must be performed to determine what muon energies deposit the same amount of energy in the SV as the proton. Use the same steps as presented in IV, except instead of varying proton energy to match the muon's energy deposition, the muon energy should be varied so the muon's energy deposition matches the proton's. This will provide a mapping from the SEU cross section of the proton energies that were tested to that of the muon energies that the proton energies correspond to.

Error propagation from energy deposition to cross section

The methods in this paper focus on matching muon and proton energy depositions. If the energy deposition of the particles match, than the critical charge and therefore the cross section for the device do as well. However, though critical charge and energy deposition are linearly related, SEU cross section and critical charge is not. [8] Thus, a change by a factor of two in the charge deposited in the device SV does not correlate to a factor of two change in SEU cross section. In order to correlate the two errors, a

functional relationship between SEU cross section and energy deposition must be found. This paper will not go into the details of how to do so, though Peterson *et al.* provide an excellent discussion of the effectiveness of fitting parameters. [9]

Determining the muon upset rate using the methods

First, the particle environment should be quantified. The muon flux at sea level should be transported through any materials above the device (such as the ceiling). Note that while only the spectrum of the low energy tail of the particles changes significantly, this is the region a designer should be most concerned about given higher probability for low energy stopping muons to cause an upset. Nonetheless, a first order calculation is sufficient for these purposes since the spectrum changes only slightly with increasing amount of material before the device. However, variation in this transport will result in slightly different upset rates in the environment. Fig. 8 shows the difference between the sea level muon spectrum before and after being transported through 10 cm of concrete. In the range the muons are likely to be stopping there can be a significant change in the muon flux from sea level. For the most part angular effects can be simplified. Since muons originate in the upper atmosphere, the angular distribution of the muons is heavily weighted as being normal to the ground. Simulations and tests can therefore be performed with the muons normally incident on the device at whatever angle it may be at in practice.

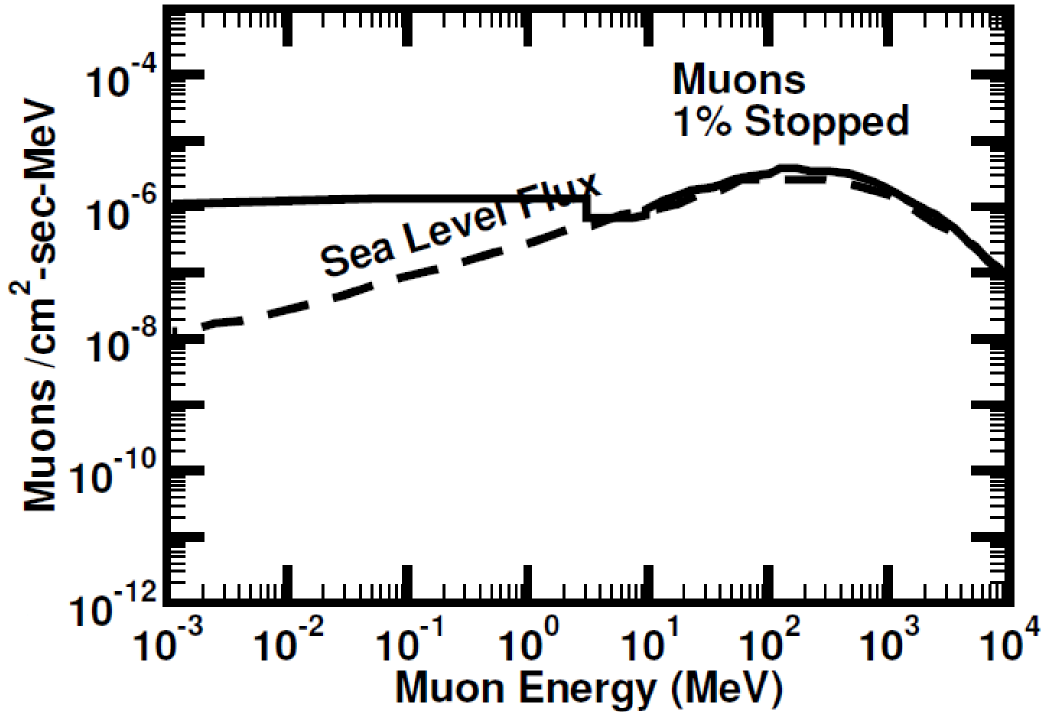

Figure 8: Muons at sea level and after being transported through 10 cm of concrete. [2]

Once the muon flux is determined, the muon energies the part should be tested for can be derived from the BEOL. On the low end, any muon whose energy is great enough that it reaches the SV through the BEOL should be tested. MRED or TRIM simulations can be used to determine which muons pass through the BEOL and reach the SV. The maximum energy of muon tested is best determined by the maximum energy of the proton beam used. In other words, the maximum muon energy tested should simply be the maximum energy of the proton beam. If this is impractical, working from the lowest energies and concentrating on muons stopping in the device is the best option since these are more likely to have a large upset cross section. Muons of significantly higher energy than those stopping in the SV will deposit very little energy within the SV. Once the experiment is done, if the highest energy protons tested show that upsets are significant for the corresponding muon energies then higher muon energies must be considered for the part. It is recommended that the number of muon energies chosen between the upper and lower bounds of the experiment be enough to interpolate between them using the Weibull

distribution. In the region where the muons are stopping in the device, many data points should be taken since this is the region of greatest slope in the SEU cross section vs. muon energy curve. For higher energy muons, the change in SEU cross section is small between energies so fewer data points need to be taken.

Now that the muon flux incident on the device and the muon energies the part is susceptible to are determined, the methods presented before in the paper should be used to determine the proton energies whose energy depositions match the muons for testing. Then, proton tests are performed to determine the upset cross section for each of those muon energies. Interpolating the cross section between muon energies gives SEU cross section as a function of muon energy. Integrating muon flux multiplied by the muon SEU cross section as a function of muon energy gives the overall upset rate for the device in the expected environment.

CHAPTER V

PROTON TESTING

There are several considerations while testing a device for vulnerability to proton induced upsets. [10] If the device is expected to be vulnerable to SEUs, small fluencies can be used. However, for more tolerant devices it may be necessary to perform large fluence tests to get good statistics, in which case replacement parts should be rotated in before total dose effects become a concern. In this work we are mostly concerned with low energy protons (which correspond to low energy muons). For example, the Pelletron at Vanderbilt can produce proton energies between 500 keV and 4 MeV corresponding to velocity matched muon energies ranging from 56 keV to 450 keV. The depth a 4 MeV proton can penetrate pure SiO_2 is 148 um according to SRIM. This gives an idea of the absolute maximum BEOL thickness that can be tested in this Pelletron beam. However, the maximum BEOL that can be tested while maintaining a proton energy of 10% of 4 MeV within the sensitive volume is 23 μm of SiO_2, calculated using the Bragg peak testing methods presented above. At the low end, the maximum BEOL useable for 500 keV ± 10% is 0.75 μm SiO_s. Thus if the BEOL of the test device is under 1.5 μm of SiO_2, the device can be fully characterized in the energy ranges produced by the Pelletron with no significant energy losses in the BEOL. Of course, degraders can be used to further decrease the energy, but this comes at the expense of the full width half max of the beam energy spectrum.

Dosimetry is provided for proton tests at the Pelletron through the use of a backscatter detector. The fluence in the chamber is determined from the number of particles deflected off a gold foil that strike a surface barrier detector. Connections into the chamber are provided as BNC connectors. Additional connections can be added, but since the chamber is held under vacuum; cables must be designed to ensure the vacuum holds. Allow the staff a couple of weeks to ensure that these can be made in time. Additionally, check beforehand that the test board can fit within the end chamber and to minimize the

volume of cables. A laser alignment system is available for ensuring the device is mounted properly in the beam.

Proton upset cross section is typically determined by placing the device in the beam at normal incidence at nominal bias and measuring the number of upsets per unit fluence. After the base measurement, other angles of incidence and biases can be tested. These tests can substitute for muon test in any case, but care must be taken that any change in angular dependence doesn't change the amount or composition in the particle track or the LET of the proton may begin to differ from the muons. Fig. 9 shows a general method for proton hardness assurance testing.

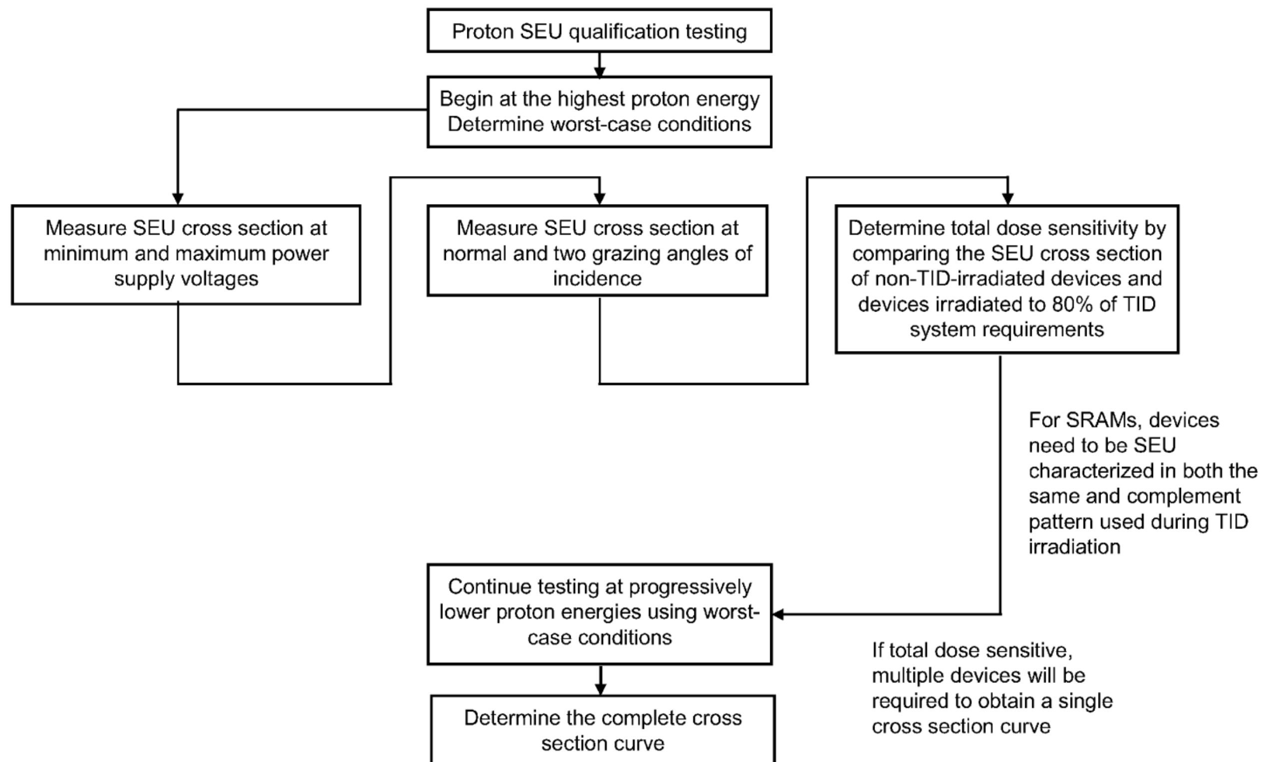

Figure 9: Outline of proton hardness assurance testing procedure, which should be followed carefully for the proton tests part of either method

Further information can be perused in the paper presented by Schwank *et al.* that outlines proton hardness assurance testing procedures. [10]

CHAPTER VI

SIMULATION CONCERNS USING MRED

Using MRED for the simulations is recommended. Sample code for the application in the following section is provided in Appendix I. Simulations should be performed on a device model that accurately approximates the geometry as closely as possible. One note of difference between simulations and experiments is the use of a point source in simulations. It is highly discouraged to use a point source since for like velocity muons and protons the lateral straggling will be very different. For certain combinations of BEOL depth and SV volume there will be a discrepancy due to the straggling. Thus, it is recommended that the user always choose directional flux (an option that provides a beam randomly sampled across a plane orthogonal to the Z axis located at the edge of the world on the negative Z axis). This averages out the lateral straggling and gives good agreement between muon and proton runs for small volumes. During testing, as long as the beam spot is uniform and much larger than the device the straggling will not have an effect on the result.

Another concern with simulations is ensuring that adequate statistics are reached during simulation. For small SVs located at the center of a large block of material, the directional flux option seems to causes an issue. Consider a ratio of a $(100\ nm)^2$ SV to a $(1\ \mu m)^2$ total area of the device. An incident particle then only has about a 1% change to directly strike the SV. Since such a large number of strikes to not be direct hits, it is important to consider this when designing the simulation. However, as shown in the validation section, delta rays from indirect hits do average out to maintain the same energy deposition between protons and muons in the same conditions as for direct hits. It is best to trim as much of the device down to just the SV and enough surrounding material to account for the delta rays. Having the total device area be double that of the SV will typically be acceptable.

The connection between LET and upset cross section is understood to be related approximately by the Weibull distribution. Peterson *et al.* do an excellent job explaining how the relationship between LET and SEU cross section is derived. [9, 11] For the purposes of this work, the important point is that cross section as a function of LET is independent of the incident particle. Since the energy deposition in the SV is a function of the LET, if the energy deposition in the SV is the same the upset cross section should be the same. This is consistent with the expectation that the critical charge generated is proportional to the deposited energy as presented before. Thus, if the energy deposition is the same for a given device between muons and protons of the same LET, then the cross section will be the same as well. MRED can be used to designate charge collection efficiencies and accurately calculate the upset cross section for a device, but this is not necessary to use the methods presented in this work. Knowing the energy deposition is the same alone is enough to compare muons and protons. However, refer back to chapter IV for a discussion on error propagation between energy deposition and SEU cross section.

CHAPTER VII

VALIDATION

The first step to validate our procedure was to show that for matched proton and muon velocities the energy deposition is the same. The model used in these simulations consists of a thick Si BEOL that slows the particle as it nears the sensitive volume. The sensitive volume itself is constructed of a grid of small detectors evenly spaced in x and y. Finally, a small Si layer is placed behind the sensitive volume. This model is shown in Fig. 10.

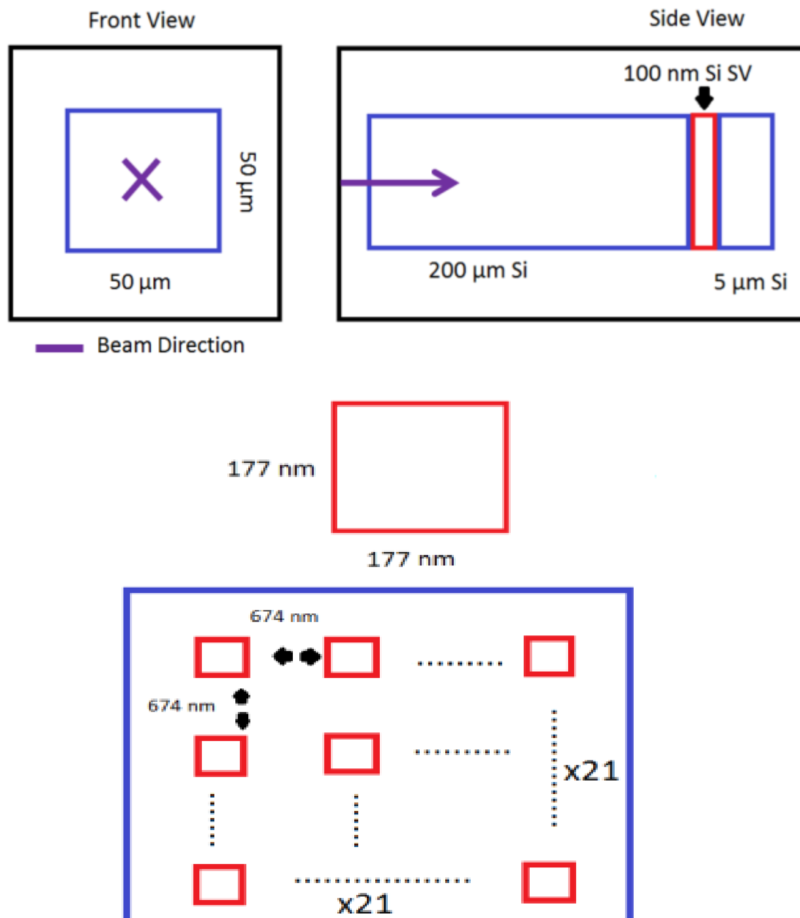

Figure 10: Device geometry used for several of the examples in Validation-Simulation

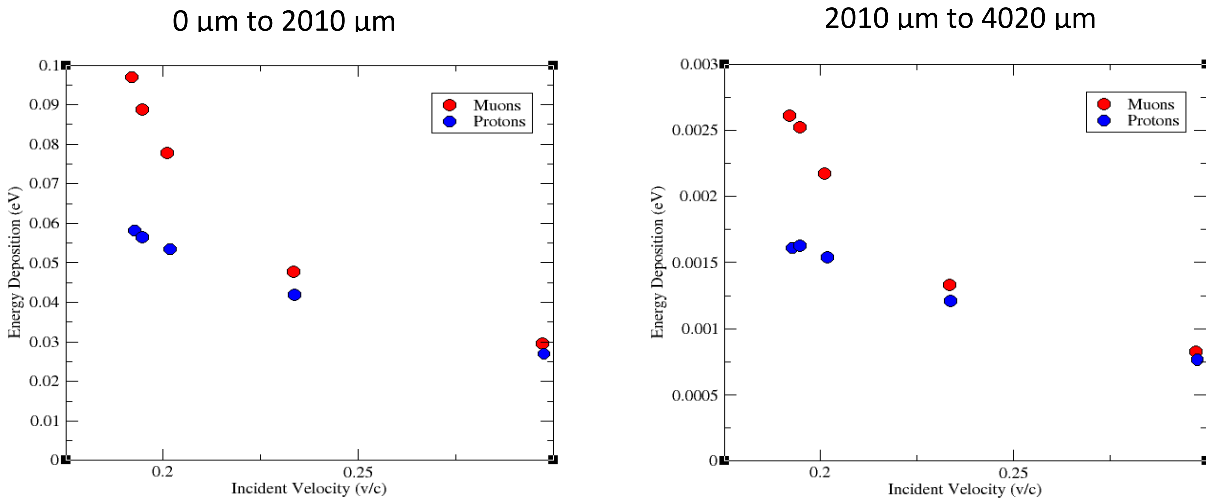

Figure 11: Results demonstrating the relationship between average energy deposition per cell and incident velocity for 12 million events. Above each graph, the ranges of distances from the beam center of the detectors being examined are presented.

This model is a simple one, but this method of verification through simulation has been shown in previous work to model energy deposition well with protons. [2] The results from these simulations are shown in Fig. 11. At low velocities near the muon Bragg peak, almost a factor of two between the muon and proton energy depositions is observed. However, as the velocity increases, the energy depositions begin to converge. Thus, the muon and proton energy deposition in each cell match at high incident velocities when the muon penetrates far beyond the Bragg peak. Since these particles will be depositing the same amount of charge, this simulation provides evidence that Method 1 will predict muon energy deposition if the conditions are met.

Another question Fig. 10 attempts to answer is if the contribution of delta rays, secondary electrons from the incident ion strike, can cause proton and muon energy depositions to disagree. As can be observed from the plots, the protons accurately predict the muon energy deposition even far outside the ion straggling range for muons if the sensitive volume remains outside the Bragg peak. These results

demonstrate that Method 1 can work even for upsets caused by secondary particle strikes. The energy depositions do not match exactly, which is expected since the devices more than 2010 µm from the center are only experiencing small numbers of delta rays. However, the trend is the same, and the protons are still predicting the muon energy deposition closely at high velocities in these outlying regions.

The simulation used to validate Method 2 uses a similar model to Fig. 10. Several simulations were performed to determine the optimum proton energy to match the LET to the muon LET for incident muons with energy of 2 MeV. Note that at 2 MeV, by time the muons penetrate to the device's sensitive volume depth they are within the Bragg peak and velocity matching does not produce similar LETs for muons and protons. The proton energy determined to produce the best match was 12.5 MeV, corresponding to a proton much slower than the 2 MeV muon. The sensitive volume depth was varied from 100 nm to 50 µm and plotted against the ratio of muon and proton energy depositions in Fig. 12.

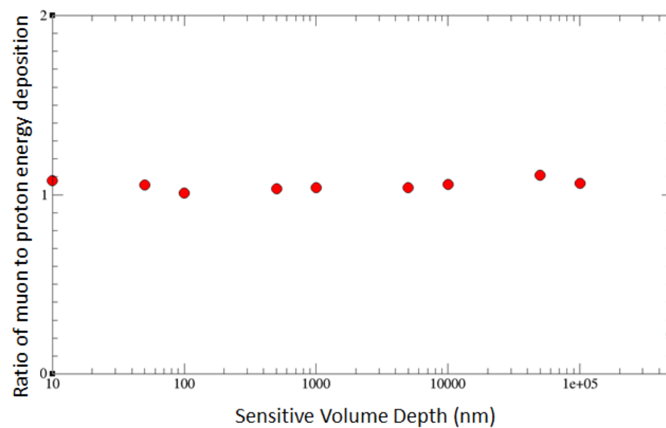

Figure 12: Ratio of proton and muon energy depositions as a function of sensitive volume depths

The approximation works up to an extremely large sensitive volume depths compared to submicron technology nodes. Due to the nature of the structure of the Bragg peak, the muon's LET changes significantly over the course of the entire depth while in the Andersen-Ziegler region. However, since

the maximum penetration depth is so large compared to the sensitive volume depth, the LET does not change significantly within the sensitive volume. For extremely large sensitive volumes above 10 µm, the LET will change significantly within the sensitive volume. However, this shows that Method 2 works very well for sensitive volume sizes corresponding to submicron technology.

Finally, an analysis of the lateral straggling of protons is presented to demonstrate the impact it can have on the energy depositions of the material. Consider a device with a $(100\ nm)^3$ cube Si SV, a 1 μm^2 square face, and a 10 µm SiO_2 BEOL. As is shown in the sample simulation section, a 1 MeV muon has nearly constant LET in the SV and thus be reasonably closely matched with a same velocity incident 8.9 MeV proton. Using the dithered point source option and the directional flux Table 1 was constructed.

MRED Source Option	Ratio of Proton to Muon Energy Deposition in the SV
Directional Flux	0.91
Dithered Point Source	22.5

Table 1: Change in consistency of ratio proton to muon energy deposition depending on source

It is apparent then that the directional flux option produces a result more consistent with theory than the dithered point source. The reason for this discrepancy is related to muons straggling away from the SV in the BEOL when using a point source. Since many of these do not strike, the average muon energy deposition is lower. In the directional flux case, every track has about the same chance of striking the SV since the strike location is randomly chosen. It is therefore recommended to always use the directional flux option.

CHAPTER VIII

SAMPLE SIMULATION AND USAGE OF THE METHODS

Assume a device with a 10 µm pure SiO_2 BEOL and a $(100\ nm)^3$ cubic SV of pure Si that needs to be tested for susceptibility to 250 keV, 500 keV, and 1 MeV muons. A diagram is provided in Fig. 13. All the energy depositions between the muon runs and the proton runs must be within 10% for the proton energy to be considered acceptable for laboratory testing. The model was constructed in MRED and the simulation code presented in Appendix I. Using the formula from Eqn. 1, the velocity matched proton energies were calculated to be as in Table 2.

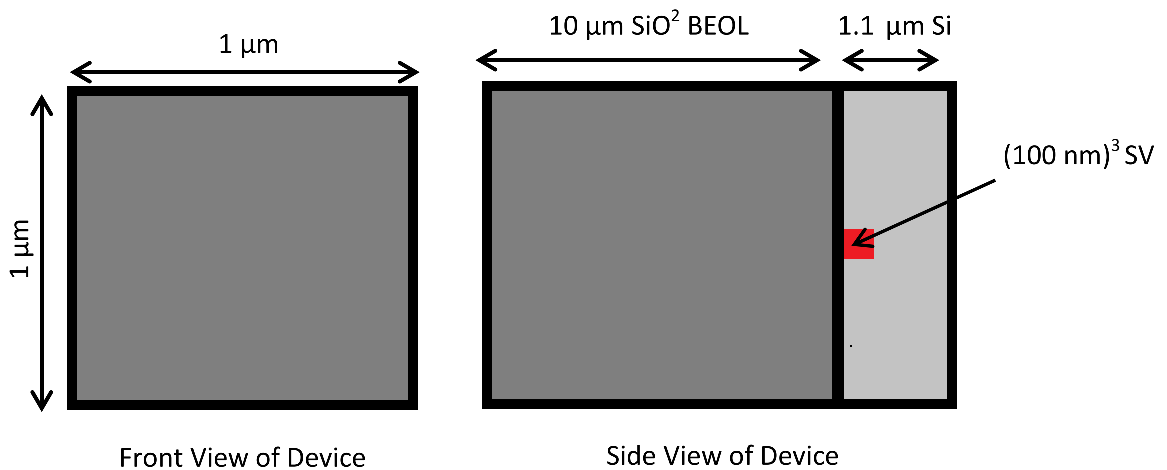

Figure 13: Model of the device used in the sample simulations

Muon Energy	Proton Energy
250 keV	2.2 MeV
500 keV	4.5 MeV
1 MeV	8.9 MeV

Table 2: Velocity matched proton energies for given muon energies

The particle energy was simulated using a directional beam flux normally incident to the BEOL of the device. 90,000 ion strikes per energy were simulated, which gives reasonable statistics for strikes in the sensitive volume. Penelope Fortran was turned on to guarantee good accuracy within the sensitive volume at low energies.

For the 250 keV muons, the particles are not capable of penetrating the 10 µm BEOL. While this seems like a trivial example, notice that the 2.2 MeV protons are capable of penetrating the BEOL and will deposit energy in the SV. Therefore, this cautionary example reminds the user to ensure that the muon penetrates the BEOL before using either Method 1 or 2. Without performing at least a SRIM simulation to check the penetration depth and going straight to the beam to measure the proton SEU cross section, the part may seem vulnerable to muon upsets when it is not.

The 500 keV run demonstrates that at low energies it is possible to get good agreement between muon and proton energy runs using Method 2. Due to being close to the Bragg peak, between the 4.5 MeV proton run and the 500 keV muon run the ratio of proton to muon energy depositions is 0.82. Assuming that an agreement of 10% or better is needed, the accuracy of the measurement must be improved by choosing a smaller proton energy. Decreasing the incident energy of the proton will increase its LET. The results from several tests are presented in Table 3.

Proton Energy (MeV)	Ratio of Proton to Muon Energy Deposition in the SV
4.5	0.82
4.25	0.87
4.0	0.93
3.75	0.98
3.5	0.99
3.25	1.09
3.0	1.14

Table 3: Comparison of proton and muon energy deposition in the 500 keV muon case

So even though direct velocity matching produces a large error, using MRED to tune the LET of the incident proton until it matches that of the muon is an effective method. A proton with energy between 3.25 MeV and 4.0 MeV will deposit about the same energy into the SV as a 500 keV muon. Note also that for the Pelletron at Vanderbilt this is a reasonable range, so accurate muon tests can be done easily in this case.

Finally, consider the 1 MeV muon run. Initial SRIM simulations in SiO_2 show the muon LET to be 40.8 MeV-cm^2/g with a range of 199 µm. This confirms that the particle will penetrate the BEOL and have an energy of about 0.90 MeV. In this case MRED simulations can be skipped and 8.9 MeV protons can be used for testing per Method 1. However, to highlight a few potential options further simulation results from MRED are presented in Table 4.

Proton Energy (MeV)	Ratio of Proton to Muon Energy Deposition in the SV
8.9 MeV	0.91
8.0 MeV	1.01
7.0 MeV	1.16

Table 4: Comparison of proton and muon energy deposition in the 1 MeV muon case

Table 5 shows validation that the approximation using SRIM carries over well into energy deposition in MRED. For a 10% decrease in LET over the SV, there is about a 9% decrease in energy deposition. It is reasonable then to use SRIM to guestimate the proton energy in these higher energy cases, as energy deposition should be approximately linear with LET.

Using Method 1 may be risky since it will always underestimate the muon energy deposition. For certain high reliability applications where it is better to overestimate the energy deposition, always employ Method 2 over Method 1. For example, in the 1 MeV muon case the 8.9 MeV proton gives a good agreement, but decreasing the energy to 8.0 MeV gives better agreement and slightly overestimates the

muon energy deposition. It may even be wise to decrease to 7.0 MeV to give a very sure margin of error to ensure good accuracy when using these methods.

The proton energies derived here would be selected and used to test the part for muon susceptibility. Specifically, the 250 keV muon does not need to be tested since it does not penetrate the BEOL of the device. The 500 keV muon should be substituted with a proton energy of 3.5 MeV, and the 1 MeV muon with a proton energy of 8.9 MeV. With these substitutions, the muon energy deposition for this theoretical part can be approximated for all cases to within 10%.

CHAPTER IX

INHOMOGENEOUS BEOL STRUCTURES

Certain BEOL compositions complicate the usage of Method 1. Specifically, very dense metals interspaced within the BEOL can cause nuclear reactions to become a factor, greatly impacting the observed energy deposition. Additionally, LET is not constant for all materials, even if it is normalized to density. [12] The structure in Fig. 14 was used to demonstrate the hazards of these effects. The size of the tungsten plug in this structure is greatly exaggerated in order to instigate nuclear reactions. The device's BEOL was specifically designed to instigate nuclear reactions. In additions, the sigma bias parameter that controls the nuclear reaction rate was turned up to 200. Thus, the contribution of the nuclear reactions is greatly increased in these simulations.

Figure 14: Inhomogeneous stack of materials used in the following simulations [12]

The results for muon and proton simulations are presented in table 6. Note that each muon energy is matched to a proton energy with approximately the same velocity.

Muon Energy (MeV)	Proton Energy (MeV)	Ratio of Proton to Muon Energy Deposition in the SV
0.25	2.2	1200
0.30	2.7	93
0.35	3.1	0.76
0.40	3.6	0.70
0.45	4.0	0.80
0.50	4.4	0.84

Table 6: Ratio of proton to muon energy depositions for select energies incident on the device presented in Fig. 14

Obviously the 250 keV and 300 keV cases are stopping slightly before the SV and the delta rays are depositing all the energy. The interesting case is the difference in energy depositions between the 0.35 and 0.40 MeV energy cases. This can be attributed to an increased contribution of the primary particle inside the deep 2.25 µm SV. These larger SVs have a larger muon energy range where the particle is stopping within them compared to smaller SVs. Thus, the user should be aware in these cases that completely stopped particles may deposit less energy than particles stopping within the SC. Note that the 0.50 MeV particle would easily be velocity matched in a pure SiO_2 BEOL, but the contribution of the dense tungsten requires a higher energy particle to match the particles velocity after the BEOL. Both methods still work in their respective cases, but the user should be aware that different BEOL compositions can cause drastic changes in the energy deposition profile. Even with the contributions of nuclear reactions and variations of LET within materials, a valid comparison can be made between muons and protons from the data in Table 6.

CHAPTER X

METHOD 2 WITH TRIM

This section will demonstrate how to use TRIM to shortcut Method 2, intended for users who either do not have access to MRED or simply want to perform these calculations quickly. Consider that like velocity muons and protons have identical energy, so if the particles velocity is matched after the BEOL then the energy deposition profiles will be identical. This is especially true for shallow SVs. However, TRIM reports losses due to ionization in eV/Angstrom with no normalization to density. As such, instead of normalizing velocity, this procedure will attempt to normalize losses due to ionization within the SV. To illustrate this example the same simple device structure from Fig. 13 will be reused.

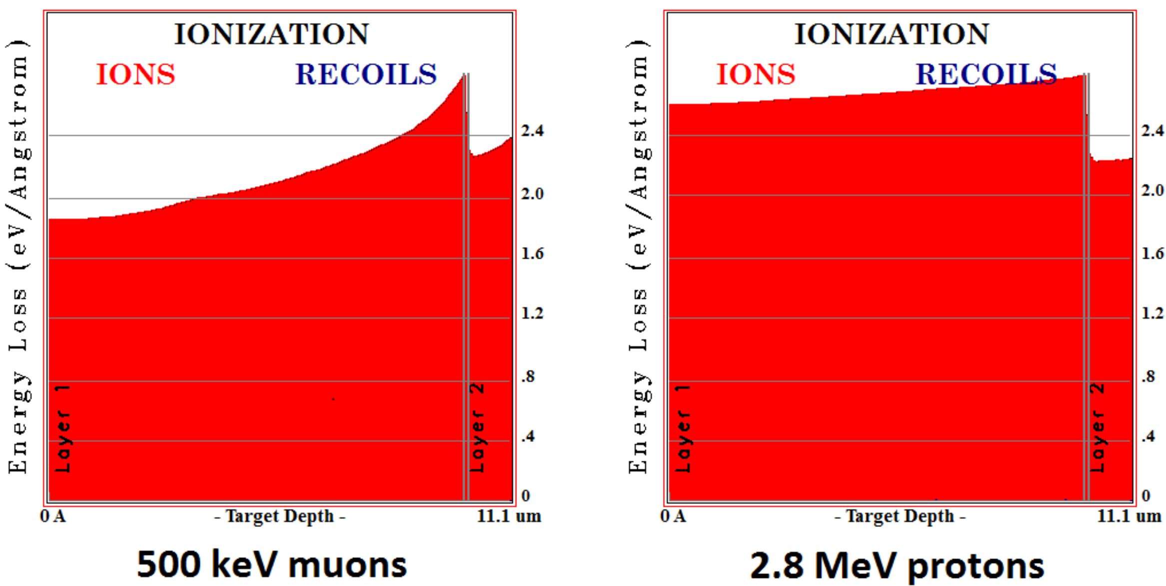

Figure 15: TRIM outputs comparing ionization in the structure illustrated in Fig. 13 for 500 keV muons (left) and 2.8 MeV protons (right). Even though the energy deposition profiles across the device are different, within the SV (layer 2) the ionization is about the same.

Fig. 15 shows the results for a TRIM simulation by using a 0.113 AMU hydrogen ion as a proxy for a muon. It has the same charge and mass as a muon, and as such behaves similarly. The muon has an energy of 500 keV, and the proton (a hydrogen ion with mass 1.008 AMU) has an energy of 2.8 MeV. This energy was found by comparing several proton energies' ionization to the muon's until they were approximately the same within the SV. Note that the proton energy chosen is significantly less than the one chosen from MRED simulations. This discrepancy tends towards overtesting the device; according to an MRED simulation on the same volume with a $(100\ \text{nm})^3$ SV , a 2.8 MeV proton deposits 1.20 times as much energy as a 500 keV muon. The proton testing will therefore overestimate the upset cross section according to the relationship between SEU cross section and energy deposition. Because of the nature of terrestrial muons, ground based SEU tests will often involve testing for the range on energies in the low energy tail. As such, across all muon energies tested, the upset cross section will be shifted slightly higher for given muon energies. From a reliability standpoint, if testing efficiency is a concern, using TRIM in this example provides a faster way to test for muon susceptibility that has the disadvantage of overtesting the part by a significant, unknown margin.

ICRU report 49 provides some insight into the discrepancy between the MRED and TRIM simulations. [13] According to the report, SRIM has an error from experimental values of 0.4 ± 5.6 (normalized mean ± normalized standard deviation) for hydrogen atoms incident on a combination of 27 compounds. Assuming that the bootstrapped muons simulated using 0.113 AMU protons have the same error, the compounded mean and standard deviation for the difference is 0 ± 7.84 for velocity matched particles. Even in this case, the 0.2 error seen above is easily within this combination of mean and standard deviation. Note also that the method used to calculate muon energy deposition in TRIM likely has even more error. Overall, it is not surprising that TRIM simulations do not agree fully with MRED simulations.

Based on the details in ICRU report 49, the user would be wise to be sure that the large variance in TRIM simulations will not impact the results from the muon simulations. The error should be propagated from the variance from TRIM to the cross section for the device as discussed in chapter IV. If the error in the SEU cross section for the device is too high over the desired ranges, then MRED or another program should be used for simulations. There are several options besides TRIM that can use the same techniques presented in this section to shortcut Method 2. Many are outlined as part of ICRU report 49. Another powerful tool is CRÈME-96, which can be used in a similar vein as MRED for producing results. [14, 15, 16]

CHAPTER XI

FUTURE WORK

The immediate future of this project will revolve around producing experimental results to validate the methods above more completely. A 28 nm technology node provided by Broadcom has recently become available for low energy muon and proton testing and will be used to complete the work started in this paper. While simulations and theory provide strong evidence that the methods above produce accurate results, complete validation from experimentation is required moving forward. Additionally, cases for both Method 1 and Method 2 will be examined and compared to simulations of the part to demonstrate how to apply these methods in greater detail.

The muon tests for the 28 nm device were already performed. Based on simulations performed by Sierawski [3], the incident muon energy was derived based on scintillating material placed in front of the beam. The results are given in Fig. 16. The different sets correspond to different well structures.

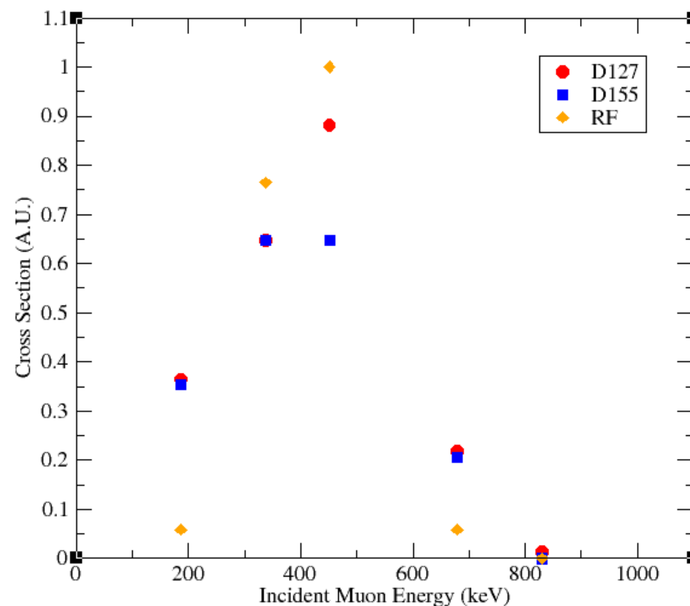

Figure 16: Muon SEU results for three Broadcom 28 nm SRAMs across several incident muon energies.

Based on these muon energies, the corresponding velocity matched proton energies would range from 1.6 MeV to 7.4 MeV. Proton tests will be performed at a future date when a test board for the 28 nm device has been completed.

Another project planned for the near future involves determining the contribution of muon decay to upsets. While it was previously stated that muon decay does not cause upsets in current technology nodes, it is possible that the energy released in these decay events could cause upsets to occur as technologies scale down. The current plan is to implement a time of flight (TOF) detector into the MRED simulations. This code will not only determine when a muon decay occurs, it will also determine the energy deposited into the sensitive volume from the event. By comparing this with critical charge measurements for the device, a model can be made to incorporate muon decay into the methods presented here.

Finally, a longer term goal is to determine the susceptibility of future technology nodes to muon upsets. This will be a long term project that will incorporate testing sub-28 nm parts for muon susceptibility with simulations to determine the most likely upset mechanisms between direct ionization and muon decay. As technology nodes shrink below 15 nm, muon induced upset rates could increase to the point that they will become a more widespread concern than now. Designers may need to consider hardening techniques for terrestrial applications that previously did not need them. The primary goal of this research will be to determine the degree to which muon induced upsets will be a concern and, if necessary, any methods by which they could be hardened against in terrestrial applications.

CHAPTER XII

CONCLUSION

In terrestrial applications, muon induced SEUs have become a larger concern for the radiation effects community as device sizes have scaled down. Muons produced from cosmic rays have been shown by Sierawski *et al.* to contribute to terrestrial SEUs in submicron parts. [2] Due to the difficulty in obtaining time on muon beams and the physical challenges presented with muon generation, a new method is introduced in this paper for determining a device's muon SEU cross section using proton tests. The method is split into two parts. First, if the device's sensitive volume is located before the Bragg peak, matching the proton's velocity to the theoretical muon's velocity predicts the muon's energy deposition adequately. However, if the muon is stopping near the sensitive volume, simulations must be used to determine the ideal proton LET to match the muon LET in the sensitive volume. Both these methods have been verified in simulations, though experimental work must be done to fully validate both methods. In addition to the theoretical validation, a brief example was presented to illustrate how the methods presented in this paper can be used to determine adequate proton energies for testing. Several common pitfalls encountered when employing the method were examined and discussed, such as the use of directional flux for the spatial sampling in MRED and the impact of heavy metals in the BEOL. A discussion on alternate simulation tools such as TRIM was included. Finally, the future of the project was outlined, from experimentally validating the methods presented here to determining the impact of muon induced upsets on future technology nodes.

REFERENCES

[1] P.E. Dodd and L.W. Massengill, "Basic mechanisms and modeling of single-event upset in digital microelectronics," *IEEE Trans. Nucl. Sci.*, vol.50, no.3, pp.583-602, Jun. 2003.

[2] B.D. Sierawski *et al.*, "Muon-Induced Single Event Upsets in Deep-Submicron Technology," *IEEE Trans. Nucl. Sci.*, vol.57, no.6, pp.3273-3278, Dec. 2010.

[3] B.D. Sierawski, "The Role of Singly-Charged Particles in Microelectronics Reliability," Ph.D. Dissertation, Dept. Elect. Eng. and Comp. Eng., Vanderbilt Univ., Nashville, TN, 2011.

[4] G. M. Marshall, "Muon beams and facilities at TRIUMF," *Zeitschrift fur Physik, C Particles and Fields*, vol. 56, pp. 226, Mar. 1992.

[5] D. E. Groom *et al.*, "Muon stopping power and range tables 10 MeV-100 TeV," *Atomic Data and Nucl. Data Tables*, vol. 78, pp. 183-356, Jul. 2001.

[6] R.A. Weller *et al.*, "Overview: Monte Carlo Radiative Energy Deposition (MRED) Code," [Online]. Available: http://129.59.140.140/wp/wp-content/uploads/weller_muri2009.pdf.

[7] S. P. Buchner *et al.*, "Variable depth Bragg peak method for single event effects testing*", IEEE Trans. Nucl. Sci.*, vol. 58, no. 6, pp. 2976-2982, 2011.

[8] C. Detcheverry *et al.*, "SEU critical charge and sensitive area in a submicron CMOS technology," *IEEE Trans. Nucl. Sci.*, vol.44, no.6, pp.2266-2273, Dec 1997.

[9] E. Petersen, "Parametric and Threshold Studies of Single Event Sensitivity," *IEEE Trans. Nucl. Sci.*, vol.54, no.4, pp.1392-1405, Aug. 2007.

[10] J.R. Schwank *et al.*, "Radiation Hardness Assurance Testing of Microelectronic Devices and Integrated Circuits: Test Guideline for Proton and Heavy Ion Single-Event Effects," *IEEE Trans. Nucl. Sci.*, vol.60, no.3, pp.2101-2118, Jun. 2013.

[11] E. Petersen *et al.*, "Rate predictions for single-event effects - critique II," *IEEE Trans. Nucl. Sci.,* vol.52, no.6, pp.2158-2167, Dec. 2005.

[12] K. Warren *et al.,* The contribution of nuclear reactions to heavy ion single event upset cross-section measurements in a high-density SEU hardened SRAM*,"* *IEEE Trans. Nucl. Sci.,* vol.52, no.6, pp.2125,2131, Dec. 2005.

[13] D. Jeasy, "ICRU Report 49, Stopping Powers and Ranges for Protons and Alpha Particles", Medical Physics, 21, 709-710, 1994, doi:http://dx.doi.org/10.1118/1.597176.

[14] A.J. Tylka, J. H. Adams, Jr., P. R. Boberg, B. Brownstein, W. F. Dietrich, E. O. Flueckiger, E. L. Petersen, M. A. Shea, D. F. Smart, and E. C. Smith, "CREME96: A Revision of the Cosmic Ray Effects on Micro-Electronics Code", IEEE Trans. Nucl. Sci., vol. 44, no. 6, pp. 2150-2160, Dec. 1997.

[15] R.A. Weller, M. H. Mendenhall, R. A.Reed, R. D. Schrimpf, K. M. Warren, B. D. Sierawski, and L. W. Massengill, "Monte carlo simulation of single event effects," IEEE Trans. Nucl. Sci., vol. 57, no. 4, pp. 1726-1746, Aug. 2010.

[16] Marcus H. Mendenhall and Robert A. Weller, "A probability-conserving cross-section biasing mechanism for variance reduction in Monte Carlo particle transport calculations", Nucl. Inst. & Meth. A, Volume 667, 1 March 2012, Pages 38-43, doi:10.1016/j.nima.2011.11.084.

APPENDIX

Sample MRED Code used for simulations in chapter VIII

```
import sys, numpy, cPickle, G4Support
from optparse import OptionParser

def SingleEventCallback(evt):

	evtWeight=mred.evtAct.GetEventWeight()

	if options.exportTracks:
		idx=commonHistogram.index(Edep)
		counts=commonHistogram.y()[idx]
		if counts <=5.0:
			seeds=mred.random_seeds
			print 'E=%g(%d,%d)' %(Edep,seeds[0],seeds[1])
			sys.stdout.flush()
			if mred.hdf5.write_ouput_files:
				mred.hdf5.writeEvent(evt)

	if options.enableDx:
		mred.dx.displayMredEvent(evt)
	if options.enableSUV:

	PyG4Core.CastEventAction(PyG4Core.RunManager.GetRunManager().GetUserEventAction
()).DrawEvent(evt)

def PostProcess():

	LET=None

	if not mred.gun.energy_spectrum:
		LET=mred.LET(mred.gun.particle,'silicon',mred.gun.energy)

	density=mred.materials.materials_dict['silicon'].GetDensity()/(g/cm/cm/cm)
		print 'finished running %0.3g MeV %s (at LET=%0.3g MeV-cm2/mg) at %0.1f
tilt, %0.1f roll'
%(mred.gun.energy,mred.gun.particle.GetParticleName(),LET,options.beamTilt,options.bea
mRoll)
		print 'Overlayer Material: %s' %options.waferMat
		print 'Channel Material: %s' %options.svMat
	if mred.hdf5.write_output_files:
		if mred.gun.random_spatial_sampling=='directionalFlux':
			mred.hdf5.setFileAttribute('fluence_unit',mred.gun.fluence_unit)
			mred.hdf5.setFileAttribute('beamTilt',options.beamTilt)
			mred.hdf5.setFileAttribute('beamRoll',options.beamRoll)
		elif mred.gun.random_spatial_sampling==options.beamRoll:
			rd=mred.detCon.GetDeviceRadius()/cm
			mred.hdf5.setFileAttribute('rd',rd)

		if LET:
			mred.hdf5.setFileAttribute('LET',LET)

		mred.hdf5.setFileAttribute('nIons',options.nIons)

def CreatePartitionedSV(length = 30.*um, width = 30.*um, svDepth = 700.*nm, svMat =
'silicon', numPartitions = 1):

	sensitiveVolume = []
```

```
        for r in range(0, int(numPartitions)):
                sensitiveVolume.append(((length, width, svDepth/float(numPartitions)),
svMat, 'sd', 'sd_region'))

        return sensitiveVolume

         '''[
        #((30.*um,30.*um,5.*um),options.waferMat,''),
        #((30.*um,30.*um,options.svDepth*nm), options.svMat,'sd','sd_region'),
        #((30.*um,30.*um,5.*um),options.waferMat,'')
        ]'''

parser=OptionParser(usage='myScript [options] [script files]')
parser.disable_interspersed_args()

parser.add_option('','--
suv',action='store_true',dest='enableSUV',default=False,help='Use the Geant4 OpenGL
Viewer')
parser.add_option('','--dx',action='store_true',dest='enableDX',default=False,
help='Use the OpenDX viewer for evet-by-event viewing')
parser.add_option('','--
dx_export',action='store_true',dest='exportDX',default=False,help='Use the OpenDX
viewer to visualize the target')
parser.add_option('','--
exportTracks',action='store_true',dest='exportTracks',default=False,help='Write the
tracks of valid events to HDF5')
parser.add_option('','--
particle',action='store',dest='particle',type='str',default='mu+',help='Particle
species')
parser.add_option('','--
nIons',action='store',dest='nIons',type='int',default=100,help='The number of paticles
to run')
parser.add_option('','--
beamE',action='store',dest='beamE',type='float',default=3,help='Beam energy (MeV)')
parser.add_option('','--
beamZ',action='store',dest='beamZ',type='int',default=1,help='Beam atomic number')
parser.add_option('','--
beamA',action='store',dest='beamA',type='int',default=1,help='Beam atomic weight')
parser.add_option('','--
beamTilt',action='store',dest='beamTilt',type='float',default=0,help='tilt angle
(degrees)')
parser.add_option('','--
beamRoll',action='store',dest='beamRoll',type='float',default=0,help='Roll angle
(degrees)')
parser.add_option('','--no-
recoils',action='store_true',dest='disableRecoils',default=False,help='Enable/disable
energy deposition from scattering events')
parser.add_option('','--no-
nuclear',action='store_true',dest='disableNuclear',default=False,help='Enable/disable
energy depostion from scattering events')
parser.add_option('','--
sigmaBias',action='store',dest='sigmaBias',type='float',default=1000,help='Hadrionic
cross section bias factor')
parser.add_option('','--
rangeCuts',action='store',dest='rangeCuts',type='float',default=.50,help='Range cuts
for electrons (um)')
parser.add_option('','--
runName',action='store',dest='runName',type='str',default=None,help='Simulation run
name')
parser.add_option('','--
min_energy',action='store',dest='min_energy',type='float',default=0,help='The minimum
energy deposited in a device')
```

```
parser.add_option('','--
writeOutput',action='store_true',dest='writeOutput',default=True,help='Write hdf5
file')
parser.add_option('','--
spatialSampling',action='store',dest='spatialSampling',type='str',default='ditheredPoi
ntSource',help='Define radom spatial sampling used by the gun')
parser.add_option('','--
useFortran',action='store_true',dest='useFortran',default=False,help='Use Fortran
Penelope')
parser.add_option('','--
nbins',action='store',dest='nbins',type='int',default=4096,help='Number of histogram
bins')
parser.add_option('','--
binSpacing',action='store',dest='binSpacing',type='float',default=600, help='Energy
between bins (eV)')
parser.add_option('','--
svDepth',action='store',dest='svDepth',type='float',default=100,help='Sensitive volume
Depth (nm)')
parser.add_option('','--
logBin',action='store_true',dest='logBin',default=False,help='Use logarithmic
binning')
parser.add_option('','--
svMat',action='store',dest='svMat',type='str',default='silicon',help='Define the
senistive volume material. Defaulted to silicon')
parser.add_option('','--
waferMat',action='store',dest='waferMat',type='str',default='silicon',help='Define the
wafer material. Defaulted to silicon')
parser.add_option('','--
numPartition',action='store',dest='numPart',type='str',default='1',help='Defines the
number of partitions in the sensitive volume')
parser.add_option("", "--rows", action='store', dest="nRows", type="int", default=20,
                  help="The number of device rows")
parser.add_option("", "--cols", action='store', dest="nCols", type="int", default=20,
                  help="The number of device columns")
parser.add_option("", "--tech", action='store', dest="tech", type="float",
default=45.0,
                  help="The scaling factor for the sensitive volume model")

(options, args)=parser.parse_args(run_args[1:])
print 'BATCH_VARS', dir(batch_vars)
print 'RUN_ARGS', run_args

PyG4Core.ExecuteCommand('/control/verbose 2')
PyG4Core.ExecuteCommand('/run/verbose 2')

#mred.physics.addModule('EmPenelopeQED')

if options.useFortran:
       mred.physics.module_dict['EmPenelopeQED'].SetUseFortranPenelope(True)
       mred.physics.module_dict['EmPenelopeQED'].SetPenelopeThreshold(100.*keV)
       print 'Fortran Penelope set True: Penelope Threshold = 100.*keV'

#mred.physics.addModule('HadronElastic')
#mred.physics.addModule('HadronInelastic')
#mred.physics.addModule('PiKInelastic')

if 0 and not options.disableNuclear:
       mred.physics.addModule('ScreenedElastic')
       mred.physics.addModule('NucleonHadronic')

#mred.physics.list.SetBiasPrimaryOnly(True)
mred.physics.list.SetSigmaBiasFactor(options.sigmaBias)
mred.physics.list.SetUseTrackWeighting(True)
```

```
print mred.physics.list.GetSigmaBiasInfo()

mred.physics.range_cuts=options.rangeCuts*micrometer

d=mred.setDevice('rpp')

mred.materials.enableBasicElectronicMaterials()

#if options.svMat not in mred.materials.basic_electronic_materials:
#       mred.materials.enableMaterial(options.svMat)
#if options.waferMat not in mred.materials.basic_electronic_materials and
options.waferMat != options.svMat:
#       mred.materials.enableMaterial(options.waferMat)

gan=mred.materials.enableMaterial(options.waferMat)

Si=mred.materials.materials_dict['silicon']

if not options.logBin:
       mred.setDefaultHistogram(min=1.0*eV,max=float(options.nbins)*options.binSpacing
*eV,nbins=options.nbins, type='linear')
else:
       mred.setDefaultHistogram(min=1.0*eV,max=float(options.nbins)*options.binSpacing
*MeV,nbins=options.nbins,type='log')

nCols=options.nCols
nRows=options.nRows

layers = [0]
margin=0*micrometer

#svLength=.1*micrometer  # 3*gateLength # [S-G-D]
#svWidth=.1*micrometer # gateWidth
svDepth = options.svDepth*nm
svLength = svDepth
svWidth = svDepth

#layerWidth=(nCols * 500) * nm + margin
#layerLength=(nRows * 500) * nm + margin

layerWidth = 2*um
layerLength=layerWidth
substrateDepth=10*micrometer

silicon = mred.materials.materials_dict['silicon']

print "Cell Size %g x %g x %g" % ( svWidth, svLength, svDepth )

box1=PyG4Core.G4Box("box1", layerWidth/2, layerLength/2, svDepth/2)

layers[0] = PyG4Core.G4LogicalVolume(box1, silicon, "_layer")

box2=PyG4Core.G4Box("box2", svWidth/2, svLength/2, svDepth/2)

sd=mred.detCon.sensitiveDetector("sd(%s,%s,%s)"%('0','0','0'))
lv = G4Support.LogicalVolume(box2, material=silicon,
name="lv(%s,%s,%s)"%('0','0','0'), sensitive=sd, color=(1,0,0), visible=True)
pv = G4Support.Placement(lv, "pv(0,0,0)", parent=layers[0], pos=Hep3Vector(0., 0.,
0.))

d.setLayers([
       ((layerWidth, layerLength, substrateDepth), 'SiO2'),
```

```
        mredPy.TargetLayerLV(layers[0]),
        ((layerWidth, layerLength, .1*substrateDepth), 'silicon')
        ])

#layers.append(((layerWidth, layerLength, 5*micrometer), 'silicon'))
#layers.append(((layerWidth, layerLength, .5*micrometer), 'copper'))
#layers.append(((layerWidth, layerLength, svDepth), options.svMat, 'sd', 'sd_region'))
#layers.append(((layerWidth, layerLength, substrateDepth), 'silicon'))
#d.setLayers(layers)

#d.setLayers(CreatePartitionedSV(length = 30.*um, width = 30.*um, svDepth =
options.svDepth*nm, svMat = options.svMat, numPartitions = options.numPart))

d.wafer_material=options.waferMat
d.register()

if options.useFortran:
        mred.init(peneMtlFile='PenelopeMaterials.dat',peneNewFile=False)
else:
        mred.init()

if options.disableRecoils:
        mred.physics.screened_scattering.allow_energy_deposition=False

mred.accumulate_histograms=True
mred.autogenerate_histograms=True
#mred.stpAct.SetMaxSteps(200000)

if not os.path.lexists('hdf5_output'):
        os.mkdir('hdf5_output')

if batch_vars:
        mred.hdf5.write_output_files=options.writeOutput
        mred.hdf5.include_histograms=options.writeOutput
        mred.hdf5.include_tracks=options.exportTracks
        mred.hdf5.file_path='hdf5_output/%s' %(batch_vars.runName)
        mred.hdf5.file_name='%s.%s.%03d.hdf5'
%(batch_vars.runName,batch_vars.isotime,batch_vars.index)
elif options.runName:
        mred.hdf5.write_output_files=options.writeOutput
        mred.hdf5.include_histograms=options.writeOutput
        mred.hdf5.include_tracks=options.exportTracks
        mred.hdf5.file_path='hdf5_output'
        mred.hdf5.file_name='%s.hdf5' %(options.runName)

if options.particle=='ion':
        mred.gun.setParticle('ion',options.beamZ,options.beamA)
else:
        mred.gun.setParticle(options.particle)

rsf=1
rso=-0*rsf*micrometer/2

mred.gun.energy=options.beamE*MeV
mred.gun.random_spatial_sampling=options.spatialSampling
mred.gun.random_use_device_radius=True
#mred.gun.setRandomBox()
l1 = [-rsf*layerWidth/2-rso, rsf*layerWidth/2+rso]
l2 = [-rsf*layerLength/2-rso, rsf*layerLength/2+rso]
l3 = [-rsf*(1.1*substrateDepth+svDepth)/2-rso, rsf*(1.1*substrateDepth+svDepth)/2-rso]
mred.gun.setRandomBox([l1,l2,l3])
#mred.gun.setRandomBox([[-1*nm,1*nm],[-1*nm,1*nm],[-1*nm,1*nm]])
tilt=math.radians(options.beamTilt)
```

```
roll=math.radians(options.beamRoll)

mred.gun.direction=vector3d(math.cos(roll)*math.sin(tilt),math.sin(roll)*math.sin(tilt
),math.cos(tilt))

print 'Gun Vector', mred.gun.direction

if options.enableSUV:
       mred.suv()
       mred.viewer.viewAngle(45,45)
if options.enableDX or options.exportDX:
       mred.dx.captureGeometry([mred.detCon.GetPhysicalWorld()],opacity_multiplier=1)

mred.progress_interval=options.nIons/100
mred.beamOn(options.nIons)

#--or--

#mred.runSingleEventMode(options.nIions,singleVent(callback)

PostProcess()
```